

# Perturbative application of next-to-leading order pionless EFT for $A \leq 3$ nuclei in a finite volume

Tafat Weiss-Attia<sup>1</sup>,<sup>✉</sup> Martin Schäfer<sup>2,\*</sup>,<sup>✉</sup> and Betzalel Bazak<sup>1,†</sup>

<sup>1</sup>*The Racah Institute of Physics, The Hebrew University, Jerusalem 9190401, Israel*

<sup>2</sup>*Nuclear Physics Institute of the Czech Academy of Sciences, Rez 25068, Czech Republic*



(Received 7 February 2024; accepted 13 May 2024; published 21 June 2024)

Lattice quantum chromodynamics (LQCD) calculations with physical pion mass would revolutionize nuclear physics by enabling predictions based on the fundamental theory of the strong force. To bridge the gap between finite-volume LQCD results and free-space physical observables, two primary extrapolation methods have been employed so far. The traditional approach relies on the Lüscher formula and its extensions, while a recent alternative employs effective field theories (EFTs) fitted directly to the finite volume data. In this study, we fit pionless EFT with perturbative inclusion of the next-to-leading order to finite-volume energies generated from a phenomenological  $NN$  interaction. The theory is then used to extrapolate the finite-volume results into free space as well as to predict new few-body observables. As a benchmark, we also apply the Lüscher formalism directly to the finite-volume data. Through a comprehensive analysis, we explore the characteristics of order-by-order predictions of the pionless EFT fitted within a finite volume, investigate the limitations of the different extrapolation techniques used, and derive recommended box sizes required for reliable predictions.

DOI: 10.1103/PhysRevD.109.114515

## I. INTRODUCTION

In the realm of nuclear physics, future *ab initio* predictions for low energy observables would ideally be based on lattice quantum chromodynamics (LQCD), a lattice gauge theory of quarks and gluons at low energies [1–5]. LQCD involves extensive numerical calculations performed on a finite space-time lattice, and in the limit of an infinitely large lattice size and infinitesimal spacing, it provides an exact solution to QCD. However, practical LQCD calculations are often performed with a small lattice size, where finite-volume effects come into play, and therefore require extrapolation of the results into free-space observables to give them physical meaning. At the moment, calculations with physical quark masses are not available; however, there is ongoing progress in approaching the physical point, see for example Refs. [6,7].

Several decades ago, Lüscher developed a method for extracting free space observables from finite-volume spectra of two-body systems confined in a box of size  $L \times L \times L$  [8,9]. This approach is based on the assumption of scale separation, where the potential range  $R$ , the possible binding momentum  $\kappa$ , and the box size  $L$  satisfy the conditions  $R \ll \kappa^{-1} \ll L$ . Nonetheless, this assumption may not always hold for all systems, considering the characteristic scales of the nuclear interaction and the

computational limitations of current LQCD calculations. For instance, the long-range part of the nuclear interaction has a range of approximately  $R \approx 2$  fm, while the typical deuteron binding momentum is around  $\kappa^{-1} \approx 5$  fm. Moreover, due to computational constraints, the box size in LQCD calculations is typically fixed at about  $L \approx 5$  fm. As the box size decreases, it becomes essential to include exponentially suppressed corrections [10,11]. Reference [10] demonstrates that incorporating corrections to Lüscher’s asymptotic formula allows extraction of the deuteron binding energy with high precision when using box sizes of  $L \gtrsim 10$  fm.

Finite-volume corrections in three-hadron systems were studied in Refs. [12–19]. So far, theoretical studies beyond three particles involve only systems where dominant finite-volume corrections might be described through the separation of  $N$ -body systems into two subclusters [20–22].

An alternative approach was proposed in Ref. [23], which suggests the use of effective field theory (EFT; see, e.g., [24] for a recent review). Here, the few-body Schrödinger equation is solved in the same finite volumes used in the LQCD calculations, and an EFT is fitted to reproduce the corresponding LQCD results. Subsequently, the infinite volume quantities are obtained by solving this EFT in free space. Specifically, a pionless effective field theory ( $\not{E}$ EFT) [25–28], where the nucleons are the only degrees of freedom, was utilized in Ref. [23] to analyze the nuclear spectrum obtained by the NPLQCD collaboration at a pion mass of  $m_\pi \approx 806$  MeV [29]. In later works,  $\not{E}$ EFT

\* m.schafer@ujf.cas.cz

† betzalel.bazak@mail.huji.ac.il

was employed to calculate relevant matrix elements and analyze other LQCD results [30–33].

One of the most important features of EFT is its ability to systematically improve results by incorporating order-by-order corrections. The majority of studies use only leading order (LO)  $\not{\text{EFT}}$  to extrapolate LQCD results [23,30–33]. While the LO is to be resummed, the subleading range corrections of  $\not{\text{EFT}}$  are to be included perturbatively to ensure a properly renormalized theory. In free space, higher order terms were perturbatively included in nuclear three-body systems up to  $N^2\text{LO}$  [34] and in four- and five-body nuclear systems up to NLO [35,36]. In finite-volume, the widely used particle-dimer formalism faces numerical challenges, once perturbative effective range corrections are included in the dimer propagator. As a result, an alternative scheme for effective range corrections was introduced [37,38]. Recently, Ref. [33] applied NLO  $\not{\text{EFT}}$  to analyze the LQCD spectra of two-nucleon systems [2]. In Ref. [33], the authors follow naive power-counting and implement at NLO all interaction terms with quadratic momenta nonperturbatively. Consequently, the theory faces renormalization issues due to the Wigner bound [39,40], the renormalization group invariance cannot be verified since the large cutoff limit cannot be reached, and the model independence is obscured.

In this study, we employ the power-counting scheme as used in Refs. [34–36]. The NLO contains effective range corrections, which are included through the perturbative insertion of two-body momentum-dependent  $s$ -wave terms. This allows us to access both the cutoff dependence of our two- and three-body  $\not{\text{EFT}}$  results as well as finite-volume effects induced by the fit of  $\not{\text{EFT}}$  low-energy constants (LECs) to finite-volume spectra. Calibration of LECs using finite-volume energies requires an accurate solution of the few-body Schrödinger equation in a box with periodic boundary conditions. Here we use the correlated Gaussian-based stochastic variational method (SVM), which has shown its ability to accurately capture the finite-volume effects [41,42], and serves as a reliable tool for fitting  $\not{\text{EFT}}$  to LQCD data [23,30–33]. Specifically, we use the implementation from Ref. [23], which has been further optimized and improved in Ref. [42] to obtain efficient and accurate computations in a periodic box, and which has been generalized in this work to include NLO terms as well. Due to the lack of nuclear LQCD results at physical pion mass, we artificially generate LQCD-like data. To this end, we assume that the nuclear interaction is fully described by the phenomenological Minnesota potential [43]. The extracted free-space LO and NLO  $\not{\text{EFT}}$  results are then compared to the corresponding values calculated directly from the Minnesota potential. We observe a significant improvement in the results obtained using NLO  $\not{\text{EFT}}$  in comparison to the LO results, indicating that the NLO corrections effectively account for finite volume effects. In most of the investigated systems, the NLO  $\not{\text{EFT}}$  yields

predictions with high accuracy when utilizing box sizes  $L \gtrsim 7$  fm.

The paper is organized as follows. Section II presents the Lüscher extrapolation formulas, which are suitable for both bound states and scattering states. Section III describes the  $\not{\text{EFT}}$  framework. Section IV presents the numerical tools used to solve the few-body problem, focusing on the implementation of periodic boundary conditions. An explanation of the fitting procedure for the EFT LECs is also included in this section. Our results are presented in Sec. V, followed by conclusions in Sec. VI. Finite-volume energies of two- and three-body systems calculated using Minnesota potential are listed in Appendix A. In Appendix B we include complementary  $\not{\text{EFT}}$  results.

## II. LÜSCHER METHODS

The common framework for processing the LQCD finite-volume data was introduced by Lüscher [8,9]. Lüscher established the connection between the finite-volume spectra of a two-body system, confined in a box with periodic boundary conditions, and the physical observables of the same system in free space, specifically the binding energy and phase shifts.

The first-order finite-volume correction to the binding energy of an  $s$ -wave two-body bound state in a box of size  $L$ ,  $\Delta B_2 = B_2(L) - B_2^{\text{free}}$ , is given by [8]

$$\Delta B_2 = \frac{6\kappa_2 |\mathcal{A}_2|^2}{\mu_2 L} e^{-\kappa_2 L} + O(e^{-\sqrt{2}\kappa_2 L}), \quad (1)$$

where  $B_2^{\text{free}}$  is the binding energy of the two-body system in free space and  $B_2(L)$  is the corresponding binding energy in a finite volume with a box size  $L$ . Here we set  $\hbar = 1$ ,  $\mu_2$  is the reduced mass,  $\kappa_2 = \sqrt{2\mu_2 B_2^{\text{free}}}$  is the binding momentum, and  $\mathcal{A}_2$  is the dimensionless two-body asymptotic normalization coefficient (ANC).

A generalization of Eq. (1) for an  $N$ -body bound state was given in Ref. [20]. Assuming that the lowest threshold of the system is a breakup into two subclusters and these subclusters can be treated as pointlike particles, the leading finite-size correction to the free-space  $N$ -body binding energy  $B_N^{\text{free}}$  is

$$\Delta B_N = C_N \frac{6\kappa_N |\mathcal{A}_N|^2}{\mu_N L} e^{-\kappa_N L} + O(e^{-\sqrt{2}\kappa_N L}). \quad (2)$$

Here,  $\mu_N$  stands for the reduced mass of the subclusters,

$$\kappa_N = \sqrt{2\mu_N (B_N^{\text{free}} - B_1^{\text{free}} - B_2^{\text{free}})}$$

is the binding momentum calculated from the free-space binding energies of the two subclusters  $B_1^{\text{free}}$  and  $B_2^{\text{free}}$ ,  $\mathcal{A}_N$  is the corresponding  $N$ -body ANC, and  $C_N$  is a

combinatorial factor counting the number of partitions of  $N$  identical particles into these two subclusters.

A formula suitable for the analysis of two-body scattering states was given in Ref. [9]. For a range of interaction  $R$  smaller than the size of the box,  $R < L$ , the free-space scattering amplitude in a specific partial wave can be related to the energy spectra of two particles in a finite volume, with periodic boundary conditions and a certain cubic symmetry. Assuming that all partial waves higher than the  $s$ -wave can be neglected, the  $s$ -wave phase shifts  $\delta_0(k)$  can be determined from the corresponding  $A_1^+$  finite-volume energies by applying the equation [9]

$$k \cot \delta_0(k) = \frac{1}{\pi L} S \left[ \left( \frac{Lk}{2\pi} \right)^2 \right]. \quad (3)$$

Here  $k$  is the relative momentum corresponding to the finite-volume energy  $E = k^2/m$ , with nucleon mass  $m$ .  $S(\eta)$  is given by the regularized sum [44]

$$S(\eta) \equiv \lim_{\Omega \rightarrow \infty} \left( \sum_{\mathbf{j} \in \mathbb{Z}^3} \frac{1}{|\mathbf{j}|^2 - \eta} - 4\pi\Omega \right), \quad (4)$$

running over all integer three-vectors  $\mathbf{j}$  such that  $|\mathbf{j}| < \Omega$ . The next lowest partial wave that can also affect the  $A_1^+$  finite-volume energy spectrum is the  $g$ -wave. At nuclear energies considered in this study, the  $g$ - or even higher partial-wave contributions to the spectrum are negligible, and their effect is not taken into account.

The scattering length and effective range can be obtained by fitting the extracted  $s$ -wave phase shifts with the effective range expansion (ERE)

$$k \cot \delta_0(k) = -\frac{1}{a_0} + \frac{1}{2} r_0 k^2 + O(k^4). \quad (5)$$

Using the scattering parameters, the two-body binding energy can be approximately calculated,

$$B_2 \approx \frac{1}{ma_0^2} \left( 1 - \frac{r_0}{a_0} \right)^{-1}. \quad (6)$$

### III. $\not\epsilon$ EFT UP TO NLO

An alternative approach to utilize LQCD results is to fit the  $\not\epsilon$ EFT directly to LQCD finite-volume spectra [23,30–33]. At LO, each two- and three-body  $s$ -wave channel contains one two- and three-body contact interaction term, respectively. After regularization, the contact interaction is smeared by a local Gaussian regulator

$$\begin{aligned} \delta_\Lambda(r) &= \frac{\Lambda^3}{8\pi^{3/2}} \exp[-\Lambda^2 r^2/4] \\ &= \frac{\Lambda^3}{8\pi^{3/2}} \prod_{\alpha \in \{x,y,z\}} \exp[-\Lambda^2 (r^{(\alpha)})^2/4], \end{aligned} \quad (7)$$

where  $\Lambda$  is the momentum cutoff. The regularized LO potential takes the form

$$\begin{aligned} \hat{V}^{(0)} &= \sum_{i<j} \left( C_0^{(0)}(\Lambda) \hat{\mathcal{P}}_{ij}^{[0,1]} + C_1^{(0)}(\Lambda) \hat{\mathcal{P}}_{ij}^{[1,0]} \right) \delta_\Lambda(\mathbf{r}_{ij}) \\ &\quad + \sum_{i<j<k} \sum_{\text{cyc}} D_0^{(0)}(\Lambda) \hat{\mathcal{Q}}_{ijk}^{[1/2,1/2]} \delta_\Lambda(\mathbf{r}_{ij}) \delta_\Lambda(\mathbf{r}_{jk}), \end{aligned} \quad (8)$$

where  $\mathbf{r}_{ij} = \mathbf{r}_i - \mathbf{r}_j$  is the relative coordinate between particles  $i$  and  $j$  and  $\hat{\mathcal{P}}_{ij}^{[S,I]}$ ,  $\hat{\mathcal{Q}}_{ijk}^{[S,I]}$  are projection operators into the respective two- and three-body spin-isospin  $[S, I]$  channels. Here  $C_0^{(0)}(\Lambda)$ ,  $C_1^{(0)}(\Lambda)$ , and  $D_0^{(0)}(\Lambda)$  are the LO LECs which have acquired cutoff dependence after regularization.

Moving into the next EFT order, the NLO potential contains derivatives of the contact potential, as well as counter-terms. The NLO potential takes the form

$$\begin{aligned} \hat{V}^{(1)} &= \sum_{i<j} \left( C_0^{(1)}(\Lambda) \hat{\mathcal{P}}_{ij}^{[0,1]} + C_1^{(1)}(\Lambda) \hat{\mathcal{P}}_{ij}^{[1,0]} \right) \delta_\Lambda(\mathbf{r}_{ij}) \\ &\quad + \sum_{i<j<k} \sum_{\text{cyc}} D_0^{(1)}(\Lambda) \hat{\mathcal{Q}}_{ijk}^{[1/2,1/2]} \delta_\Lambda(\mathbf{r}_{ij}) \delta_\Lambda(\mathbf{r}_{jk}) \\ &\quad + \sum_{i<j} \left( C_2^{(1)}(\Lambda) \hat{\mathcal{P}}_{ij}^{[0,1]} + C_3^{(1)}(\Lambda) \hat{\mathcal{P}}_{ij}^{[1,0]} \right) \\ &\quad \cdot (\delta_\Lambda(\mathbf{r}_{ij}) \vec{\nabla}_{ij}^2 + \vec{\nabla}_{ij}^2 \delta_\Lambda(\mathbf{r}_{ij})). \end{aligned} \quad (9)$$

At NLO, the adopted power-counting further includes a momentum-independent four-body force [35,45], which is not required in this  $A \leq 3$  study.

The model independence of our approach is ensured by requiring that both the LO and the NLO of  $\not\epsilon$ EFT are properly renormalized to low-momentum data. While the LO potential is iterated, nonperturbative inclusion of the NLO momentum-dependent (derivative) terms leads to renormalization problems caused by the Wigner bound [39,40]. To maintain a properly renormalized EFT, the NLO potential is treated within first-order perturbation theory [27].

The truncation of  $\not\epsilon$ EFT at a certain order leads to a theoretical error that reflects higher order terms not accounted for in the EFT expansion. A rough LO and NLO error estimate is  $(QR)$  and  $(QR)^2$ , respectively, where  $Q$  is the typical momentum of an observable and  $R \sim r_0$  is the interaction range. Another way to estimate the error is the residual cutoff variation, which would eventually be removed by including all EFT orders [46]. In this work, we repeat  $\not\epsilon$ EFT calculations for several values from a broad momentum range of  $1.25 \text{ fm}^{-1} \leq \Lambda \leq 10 \text{ fm}^{-1}$  which allows to assess the cutoff convergence of our results as well as to estimate the truncation error.

In a periodic box of size  $L$ , the  $\not\epsilon$ EFT potential must obey the periodic boundary conditions. Following Refs. [23,41],

this is achieved by summing over all possible translations of the box. As a result, the Gaussian regulator now has the form

$$\delta_{\Lambda,L}(r) = \frac{\Lambda^3}{8\pi^{3/2}} \prod_{\alpha \in \{x,y,z\}} \sum_{q^{(\alpha)} \in \mathbb{Z}} \exp[-\Lambda^2(r^{(\alpha)} - Lq^{(\alpha)})^2/4]. \quad (10)$$

## IV. METHODS

### A. Stochastic variational method

We solve the few-body Schrödinger equation by utilizing the SVM [47]. The total wave function  $\Psi$  is expanded on a correlated Gaussian basis [48]

$$\Psi = \sum_i c_i \hat{A} \{G_i(\mathbf{r}) \chi_{SM_s} \xi_{IM_i}\}. \quad (11)$$

$\hat{A}$  denotes the antisymmetrization operator over nucleons, and  $\chi_{SM_s}$  and  $\xi_{IM_i}$  are the spin and isospin parts of the wave function, respectively. The spatial part is given by  $G_i(\mathbf{r}) = \exp[-\frac{1}{2}(\mathbf{r}^T A_i \mathbf{r})]$ , where  $\mathbf{r}^T = (r_1, r_2, \dots, r_N)$  are the single-particle  $N$ -body coordinates, and  $A_i$  is a symmetric positive-definite matrix of size  $N \times N$ , chosen stochastically. Finally, the variational coefficients  $c_i$  and the associated bound-state energies are obtained by solving the generalized eigenvalue problem.

The total wave function in a box,  $\Psi_L$ , has to obey the periodic boundary conditions

$$\Psi_L(\dots, \mathbf{r}_i, \dots) = \Psi_L(\dots, \mathbf{r}_i + \mathbf{m}_i L, \dots) \quad (12)$$

for arbitrary integer trio  $\mathbf{m}_i = (m_i^{(x)}, m_i^{(y)}, m_i^{(z)})$ . The corresponding spatial part is then represented by a product of periodic correlated Gaussians in the  $x$ ,  $y$ ,  $z$  directions

$$G_L(\mathbf{r}) = \prod_{\alpha \in \{x,y,z\}} G_{L_\alpha}(\mathbf{r}^{(\alpha)}) \quad (13)$$

with  $(\mathbf{r}^{(\alpha)})^T = (r_1^{(\alpha)}, r_2^{(\alpha)}, \dots, r_N^{(\alpha)})$ . Following Refs. [41,42], the periodicity is achieved by summing over all box translations

$$G_{L_\alpha}(\mathbf{r}^{(\alpha)}) = \sum_{\mathbf{n}^{(\alpha)}} G_\alpha(A_\alpha; \mathbf{r}^{(\alpha)} - L\mathbf{n}^{(\alpha)}) \quad (14)$$

with  $G_\alpha$  being a correlated Gaussian function

$$G_\alpha(A_\alpha; \mathbf{r}^{(\alpha)}) = \exp\left[-\frac{1}{2}(\mathbf{r}^{(\alpha)})^T A_\alpha \mathbf{r}^{(\alpha)}\right] \quad (15)$$

and  $\mathbf{n}^{(\alpha)} = (n_1^{(\alpha)}, n_2^{(\alpha)}, \dots, n_N^{(\alpha)})$ ,  $n_i^{(\alpha)} \in \mathbb{Z}$ .

It was shown in Ref. [41] that it is beneficial to choose the  $A_\alpha$  matrices that obey

$$(\mathbf{r}^{(\alpha)})^T A_\alpha \mathbf{r}^{(\alpha)} = \sum_{i < j} \frac{(r_i^{(\alpha)} - r_j^{(\alpha)})^2}{b_{ij}^2}, \quad (16)$$

where the stochastically selected parameters  $\{b_{ij}\}_{i < j}$  reflect the relative distance between each pair of particles. Such basis functions are then invariant under center-of-mass shifts. As demonstrated in Ref. [42], the center-of-mass coordinate can be integrated out in finite-volume calculations, further simplifying the numerical computations and eliminating center-of-mass excitations.

### B. Fitting the LECs

In place of genuine physical LQCD results, we use artificially generated finite-volume data. To this end, we apply the SVM to calculate the  $A_1^+$  spectra of two and three nucleons in a periodic box, where the underlying nuclear interaction is described via the phenomenological  $NN$  Minnesota potential [43]. Using the exchange mixing parameter  $u = 1$ , this potential reproduces the experimental  $np$  spin-triplet and  $pp$  spin-singlet  $s$ -wave effective-range parameters. Furthermore, it was demonstrated that the Minnesota potential describes successfully the basic free-space properties of the deuteron, triton, and  $\alpha$ -particle [43]. The generated finite-volume data are listed in Appendix A.

Motivated by the Lüscher bound-state formulas, Eqs. (1) and (2), we show in Fig. 1 the calculated finite-volume corrections  $L|\Delta B_N|$  to the free-space Minnesota deuteron and triton binding energies. The corrections are plotted as a function of  $L$  on a logarithmic scale. The linear behavior then reveals the range of applicability of the Lüscher formulas,  $L \gtrsim 10$  fm for the deuteron bound state (filled red circles) and  $L \gtrsim 8$  fm for the triton bound state (green filled diamonds). The first finite-volume excited state in the deuteron channel (empty red squares) or both the ground and the first excited state in the dineutron channel (empty blue circles and diamonds, respectively) correspond to the finite-volume scattering states. Their  $|\Delta B_N|$  behavior, measured this time to the free-space two-body separation threshold  $B_2^{\text{free}} = 0$ , does not follow Eq. (1) but instead can be in the large  $L$  asymptotic region expanded into the  $\sim 1/L^\beta$  contributions [49].

The  $s$ -wave phase shifts are extracted from the calculated two-body  $A_1^+$  Minnesota finite-volume energies at various box sizes  $L \in \langle 3; 20 \rangle$  fm using the Lüscher scattering formula, Eq. (3). Figure 2 shows the corresponding values in terms of  $k \cot(\delta_{NN})$  as a function of  $k^2$ , which were calculated using the finite-volume ground state and the first excited state energies in the deuteron and dineutron channels. While the finite-volume energies of the first excited state are positive, the attractive nature of the  $NN$  Minnesota potential introduces negative  $A_1^+$  finite-volume

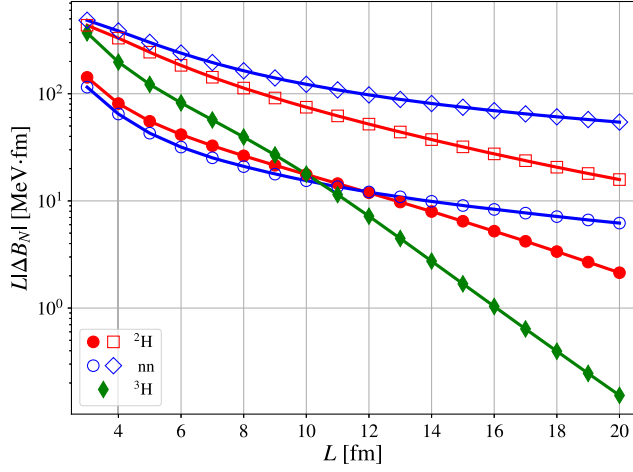


FIG. 1. The finite-volume results used to mimic LQCD data in this work. The data were obtained by solving the Minnesota potential in a periodic box with different box sizes  $L$ . Shown are the absolute values of the finite volume energy shifts  $|\Delta B_N|$ , multiplied by the box size  $L$ , as a function of the box size for the deuteron (red), dineutron (blue), and triton (green) channels. The circles and thin diamonds correspond to the finite-volume ground states. For the two-body systems, the values of the first excited state are depicted as well (squares and diamonds). The filled symbols indicate the finite-volume deuteron and triton ground states which in the large  $L$ -limit approach the free-space bound states.

ground-state energies in both two-body channels [44,49]. By approaching the free-space limit ( $L \rightarrow \infty$ ) the first excited state energies converge to  $B_2^{\text{free}} = 0$  from above, the spin-singlet ground-state energy converges to  $B_2^{\text{free}} = 0$  from below, and the spin-triplet ground-state energy converges to the free-space deuteron energy. Equation (3), used at different box sizes, yields  $k \cot(\delta_{NN})$  at different  $k^2 > 0$  (first excited states) or  $k^2 < 0$  (ground states). The latter can be understood as the analytical continuation of the phase shifts to the momenta below the two-body threshold. Once the size of the box starts to approach the range of the Minnesota interaction, the results obtained from the Lüscher scattering formula begin to deviate from the Minnesota values calculated directly in free space (black solid lines). This is apparent for phase shifts at  $k^2 \gtrsim 1.5 \text{ fm}^{-2}$  which are extracted from the finite-volume first excited state energies at box sizes  $L \lesssim 5 \text{ fm}$ .

$\not\text{EFT}$  is limited to momenta up to the one pion-exchange threshold,  $k \sim m_\pi$ . Equation (3) relates  $A_1^+$  two-body finite-volume states with energies  $E(L)$  to the free-space  $s$ -wave phase shifts with the momenta  $|k| = \sqrt{m|E(L)|}$ . As a result, we can identify which two-body finite-volume energy levels introduce high-momentum physics outside the scope of the theory and are not admissible to fit the  $\not\text{EFT}$  LECs. For the Minnesota potential, the two-body finite volume energies of the first excited state begin to surpass the breakdown scale of  $\not\text{EFT}$  for box sizes

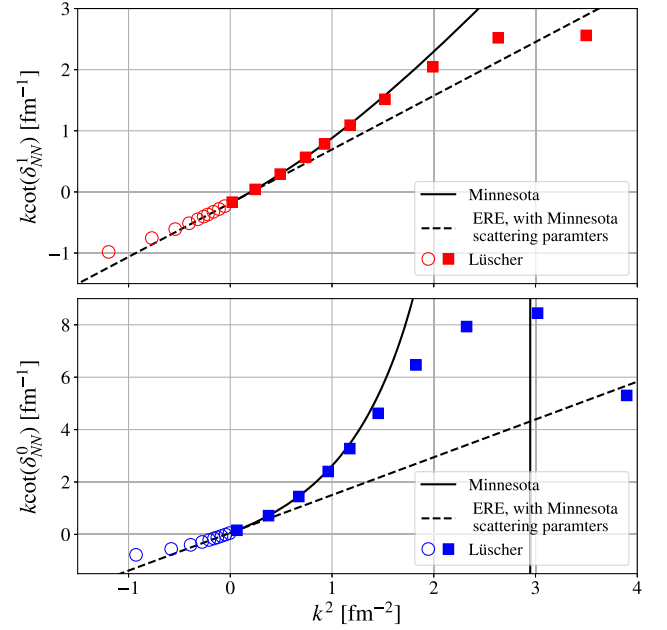


FIG. 2. The  $NN$   $s$ -wave phase shifts, presented as  $k \cot(\delta_{NN})$ , for the deuteron (upper panel) and dineutron (lower panel) channels plotted as a function  $k^2$ . We compare the phase shifts calculated directly from the Minnesota potential (black solid line) to the phase shifts extracted from the Minnesota finite-volume energies using the Lüscher scattering formula, Eq. (3). The phase shifts were calculated from both the finite-volume ground-state (empty circles) and the first-excited-state (filled squares) energies using different box sizes  $L = \{3, 3.5, 4, 4.5, 5, 5.5, 6, 7, 9, 20\}$  fm. For reference, the black dashed lines show ERE, Eq. (5), with the first two terms fitted to the “free-space” Minnesota phase shifts (black solid lines).

$L \lesssim 7 \text{ fm}$  (deuteron channel) and  $L \lesssim 8 \text{ fm}$  (dineutron channel). The same is observed at smaller box sizes  $L \lesssim 4 \text{ fm}$  for the two-body finite volume ground-state energies in both the deuteron and dineutron channels. The three-body LECs are fitted to the  $A_1^+$  ground-state finite-volume energies in the triton channel. Assuming that the box size  $L$  is sufficiently large and the finite-volume correction to the free-space deuteron binding energy can be neglected,  $E_d(L) \simeq E_d$ , the three-body finite-volume energies  $E_t(L)$  below the free-space three-nucleon separation threshold can be related to the  $s$ -wave neutron-deuteron ( $nd$ ) phase shifts with momenta  $|k_{nd}| \simeq \sqrt{4/3m|E_t(L) - E_d|}$  [50]. This suggests that by fitting the three-body LECs to  $E_t(L)$  at  $L \lesssim 8 \text{ fm}$ , we might start to introduce high momenta that exceed the breakdown scale of our theory.

To emulate usual LQCD input scenarios and to demonstrate an option how to bypass possible high-momenta of two-body finite-volume excited states, we employ two distinct approaches to fit the  $\not\text{EFT}$  LECs up to NLO:

- (1) The fitting procedure is performed by considering the finite-volume energies generated only for one size of the box  $L$ . At LO, we fit the  $C_0^{(0)}(\Lambda)$ ,  $C_1^{(0)}(\Lambda)$ , and

$D_0^{(0)}(\Lambda)$  LECs to reproduce exactly the Minnesota ground-state finite-volume energies in the dineutron, deuteron, and triton channels, respectively. The NLO two-body LECs  $C_0^{(1)}(\Lambda)$ ,  $C_1^{(1)}(\Lambda)$ ,  $C_2^{(1)}(\Lambda)$ , and  $C_3^{(1)}(\Lambda)$  are perturbatively adjusted using the LO wave functions to further reproduce the Minnesota first excited state finite-volume energies in the respective two-body spin-isospin channels, while keeping the ground-state energies at the same LO values. The remaining  $D_0^{(1)}(\Lambda)$  NLO LEC is perturbatively adjusted to keep the correct reproduction of the Minnesota finite-volume ground-state energy in the triton channel.

- (2) We employ information only from the ground-state finite-volume levels and no excited state energies are considered. At LO, we fix again the  $C_0^{(0)}(\Lambda)$ ,  $C_1^{(0)}(\Lambda)$ , and  $D_0^{(0)}(\Lambda)$  LECs by using the calculated Minnesota finite-volume energies in the dineutron, deuteron, and triton channels, respectively. However, this time, we fit each LO LEC by applying a  $\chi^2$  fit to best match two Minnesota finite-volume ground-state energies which have been calculated for two different box sizes  $\langle L \rangle \pm 1$  fm in the corresponding channel. At NLO, the two-body LECs  $C_0^{(1)}(\Lambda)$ ,  $C_1^{(1)}(\Lambda)$ ,  $C_2^{(1)}(\Lambda)$ , and  $C_3^{(1)}(\Lambda)$  are perturbatively adjusted to reproduce the Minnesota finite-volume ground-state energies in both  $\langle L \rangle \pm 1$  fm boxes exactly. Finally the  $D_0^{(1)}(\Lambda)$  LEC is perturbatively fixed to keep the LO  $\chi^2$ -fitted three-body finite-volume ground-state energy at the same LO value.

If not written otherwise, we fit  $\not\#$ EFT for each value of momentum cutoff  $\Lambda$  using different box sizes  $L \in \{3, 5, 7, 9, 11, 13, 15\}$  fm (first approach) and  $\langle L \rangle \in \{4, 6, 8, 10, 12, 14\}$  fm (second approach). To assess the cutoff dependence we consider several  $\Lambda \in \{1.25, 2, 4, 6, 8, 10\}$  fm $^{-1}$  cutoffs values. The cutoff variation is used to estimate the lower bound on the theoretical truncation error. The reported results represent the mean of calculations with different cutoffs, where the uncertainty band corresponds to the one standard deviation.

## V. RESULTS

Using the two different fitting scenarios described above, we present in this section the  $\not\#$ EFT predictions for both the deuteron, triton free-space binding energies and the low-energy  $s$ -wave  $NN$  spin-singlet,  $NN$  spin-triplet, and  $nd$  spin-quartet scattering length and effective range. Where it is possible, we benchmark the  $\not\#$ EFT results by employing the Lüscher formalism where we limit ourselves to the same finite-volume energies as were considered during the  $\not\#$ EFT fit. The resulting free-space quantities are then shown as a function of the box size and are compared

to the free-space results calculated directly from the Minnesota potential.

### A. Deuteron channel

We start with the free-space deuteron bound state energy. The corresponding value calculated directly from the Minnesota potential is

$$E_d \simeq -2.202 \text{ MeV.}$$

In the first  $\not\#$ EFT fitting scenario, we employ the finite-volume energy of the ground state (LO) and the first excited state (NLO) evaluated using the Minnesota potential at one size of the box  $L$ . The  $\not\#$ EFT free-space deuteron bound state energy  $E_d$  is then calculated by using the fitted LO and NLO LECs and solving the Schrödinger equation outside the box. The upper panel of Fig. 3 presents the corresponding LO (green) and NLO (red) results as a function of  $L$  employed during the fit. There is a significant improvement in our NLO results compared to the LO  $\not\#$ EFT prediction. For  $L \gtrsim 7$  fm the NLO  $\not\#$ EFT yields free-space  $E_d$  energies fairly close to the Minnesota value. In this box size region, the residual cutoff variation (red shaded band) suggests that the NLO theoretical error is  $\sim 3\%$ . This surpasses the expected  $\not\#$ EFT NLO truncation error, which can be estimated as  $(r_{NN}^1/a_{NN}^1)^2 \simeq 10\%$ . A possible explanation is another small parameter at play, which is related to the relevant short-range scale divided by the box size. To put it differently, the NLO LECs are calibrated using deuteron binding energy in boxes significantly larger than the short-range scales not yet considered in the EFT order, this physics is essentially already accounted for in these LECs, and no additional truncation error is introduced.

In the second fitting scenario, we consider two finite-volume ground state energies from adjacent box sizes  $\langle L \rangle \pm 1$  fm. The resulting free-space LO and NLO  $\not\#$ EFT deuteron binding energies,  $E_d$ , are shown for different  $\langle L \rangle$  in the lower panel of Fig. 3. Similar to the first case, once the NLO  $\not\#$ EFT is fitted to  $\langle L \rangle \gtrsim 6$  fm finite-volume input data, it successfully reproduces the deuteron free-space Minnesota binding energy.

The lighter-shaded bands with dotted lines depict the free-space deuteron energies, which were obtained using the  $\not\#$ EFT with LECs fitted to the finite-volume input data that introduce momenta above the one-pion-exchange threshold (see discussion in Sec. IV B). The  $E_d$  results start to deteriorate quite rapidly moving deeper into the small- $L$  region. Furthermore, our results confirm a slight advantage of the second fitting scenario which is renormalized only to the finite-volume ground-state energies and is not affected by the high momenta first excited state, which emerges already at  $L \lesssim 7$  fm.

We move now to the Lüscher approach. Due to the limitations imposed by the first fitting scenario, which

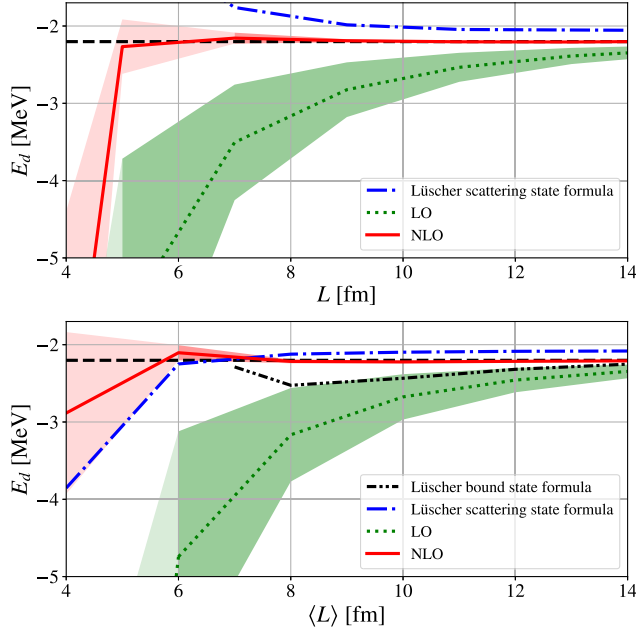


FIG. 3. The free-space deuteron binding energy  $E_d$  extracted from finite-volume energies is plotted against the varying box size  $L$  employed in the extraction. We compare different methods: In the upper panel, we use the ground-state and the first-excited-state energies from the same box size  $L$ . We show the results from Eq. (3) (blue dash-dotted line) and  $\not\{EFT}$  at LO (dotted green line) and NLO (solid red line) with LECs constrained through the first fitting scenario. In the lower panel, we use the finite-volume ground state energies from two adjacent box sizes  $\langle L \rangle \pm 1$  fm. Shown are the results obtained by fitting Eq. (1) (black dash-double dotted line), Eq. (3) (blue dash-dotted line), and  $\not\{EFT}$  at LO (green) and NLO (red) with LECs constrained through the second fitting scenario. The shaded bands in our  $\not\{EFT}$  results indicate the uncertainty induced by the residual cutoff variation within the cutoff range  $1.25 \leq \Lambda \leq 10$  fm $^{-1}$ . The lighter shaded bands reveal  $\not\{EFT}$  results where at least one LEC is fitted to a finite-volume energy which might introduce momenta above the one-pion-exchange threshold. The result calculated directly from the Minnesota potential is shown as a black dashed line.

involves finite-volume energies of the ground and first excited state within the same box, it is not possible to extract the free-space  $E_d$  via Eq. (1). On the other hand, within the second fitting scenario, we have at our disposal deuteron finite-volume ground state energies for two different  $L$ . As a result, we can use Eq. (1) and fit  $\kappa_2$  and  $\mathcal{A}_2$  to extract  $E_d$ . Interestingly, the Eq. (1), when utilized with energies from two adjacent box sizes ( $\langle L \rangle \pm 1$  fm), provides a solution only for  $\langle L \rangle \gtrsim 7$  fm and larger (see dash-double dotted black line in the lower panel of Fig. 3). To get an accuracy of about 5% one has to use  $\langle L \rangle \gtrsim 12$  fm.

Another option is to employ Lüscher's scattering state formula, Eq. (3). From the finite-volume ground state and the first excited state energies at the given  $L$  (first fitting scenario) or two adjacent ground state energies at the

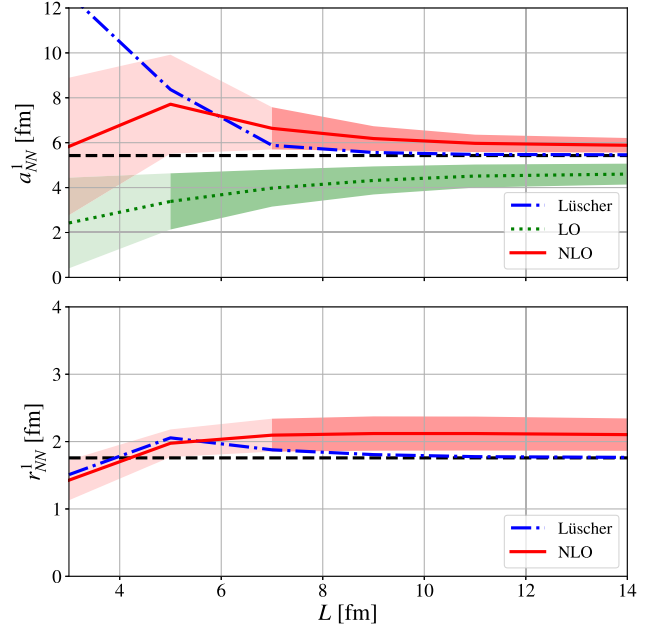


FIG. 4. Same as the upper panel of Fig. 3 but for the  $NN$  spin-triplet scattering length (upper panel) and effective range (lower panel).

average box size  $\langle L \rangle$  (second fitting scenario), we extract the  $s$ -wave spin-triplet phase shifts at two different momenta. The  $E_d$  is then obtained by fitting the ERE, Eqs. (5) and (6), to these two phase-shift points. These  $E_d$  values are shown using the blue dash-dotted line in both the upper and lower panel of Fig. 3. In the first case, the Lüscher's scattering formula yields  $E_d$  energies with  $\sim 7\%$  accuracy at  $L \gtrsim 11$  fm. In the second case, the accuracy of 5% is achieved when average box sizes  $\langle L \rangle \gtrsim 8$  fm are used. At larger boxes, the accuracy does not improve due to the truncation of the ERE, Eq. (5). Using a larger amount of finite volume excited states energies and considering higher ERE terms would likely further improve the  $E_d$  result.

The  $\not\{EFT}$  results for  $s$ -wave spin-triplet scattering parameters are shown here only for the first fitting scenario. The outcomes of the second option are similar and the corresponding results are deferred to Appendix B. The  $s$ -wave scattering parameters calculated directly from the Minnesota potential are

$$a_{NN}^1 \simeq 5.427 \text{ fm}, \quad r_{NN}^1 \simeq 1.758 \text{ fm}.$$

Figure 4 shows the predicted  $NN$  spin-triplet scattering length and effective range at LO (green) and NLO (red)  $\not\{EFT}$ , as a function of the box size  $L$  employed in the fit. The figure does not show the calculated LO effective range, since it trivially behaves as  $\Lambda^{-1}$  converging to zero in the contact limit. The blue dot-dashed lines represent  $s$ -wave scattering parameters which have been extracted by applying Lüscher's scattering formula, Eq. (3). Again, both the  $\not\{EFT}$  results up to NLO and the Lüscher predictions were

obtained using the finite volume ground state and first excited state energies from the same box size  $L$ .

The  $\not\epsilon$ EFT and Lüscher approach yield accurate predictions for the  $a_{NN}^1$  and  $r_{NN}^1$  values when utilizing box sizes  $L \gtrsim 7$  fm, although the Lüscher results converges more rapidly than the  $\not\epsilon$ EFT results, with the latter being accurate within the uncertainty band. At smaller box sizes the LO or NLO LECs are fitted to finite-volume energies which eventually introduce momenta above the breakdown scale of the theory (lighter shaded bands with the dotted lines). As might be expected this leads to deterioration of our  $\not\epsilon$ EFT results.

### B. Dineutron channel

The  $s$ -wave scattering parameters in the  $S, I = 0, 1$  dineutron channel are extracted from the finite-volume energies in a similar way as in the deuteron channel. The corresponding Minnesota scattering length and effective range values are

$$a_{NN}^0 \simeq -16.80 \text{ fm}, \quad r_{NN}^0 \simeq 2.885 \text{ fm}.$$

Both the first and the second  $\not\epsilon$ EFT fitting scenarios, outlined in Sec. IV B, yield comparable dineutron scattering predictions. Here, we discuss results related only to the first case; the results obtained through the second scenario are again included in Appendix B. Figure 5 shows the calculated LO (green) and NLO (red) inverse  $NN$  spin-singlet scattering lengths and effective ranges as a function of the box size  $L$  used throughout the fit. The inverse of the scattering length

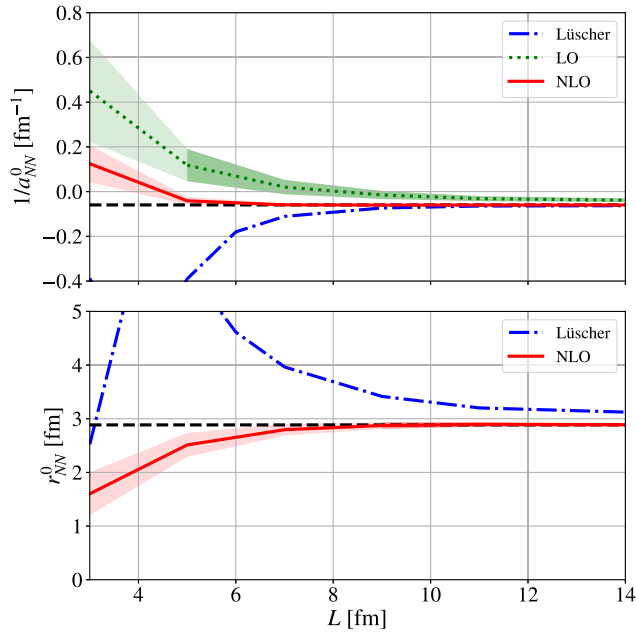


FIG. 5. Same as the upper panel of Fig. 3 but for the  $NN$  inverse spin-singlet scattering length (upper panel) and effective range (lower panel).

is selected to avoid divergences when approaching the unitary point. As seen in the figure, the results of  $\not\epsilon$ EFT demonstrate again a significant improvement from LO to NLO. Starting at the box size  $L \simeq 7$  fm and larger, the NLO  $\not\epsilon$ EFT provides predictions close to the Minnesota values with accuracy of  $\sim 1\%$ . In comparison, the size of the NLO theoretical error is roughly estimated as  $(r_{NN}^0/a_{NN}^0)^2 \simeq 3\%$ . The difference between the errors can be attributed to the presence of an additional small parameter (see Sec. VA).

The Lüscher formalism, Eq. (3), accurately predicts the scattering length for  $L \gtrsim 11$  fm, but it does not achieve the same level of accuracy for the effective range (blue dot-dashed lines). This can be explained by referring to Fig. 2, where it is evident that an accurate description of the phase shifts in this spin channel with the ERE requires consideration of the shape parameter term. Therefore, it seems that the reduced accuracy in the Lüscher prediction for the effective range is mainly due to the truncation of the ERE at second order in  $k$ .

### C. Triton channel

The three-body  $S, I = 1/2, 1/2$  channel supports the triton bound state. Its free-space energy, as calculated directly from the Minnesota potential, is

$$E_t \simeq -8.385 \text{ MeV}.$$

There is no new three-body term at NLO  $\not\epsilon$ EFT and only a single three-body energy is needed to calibrate the theory. In line with our two-body studies, we show here free-space  $E_t$  energies which have been calculated by using the  $\not\epsilon$ EFT with LECs constrained through the first fitting scenario. The  $E_t$  results obtained from the fit at two adjacent box sizes are given in Appendix B. The resulting free-space energy,  $E_t$ , is shown in Fig. 6 as a function of the box size  $L$  employed in the LEC fit. The NLO  $\not\epsilon$ EFT results approach

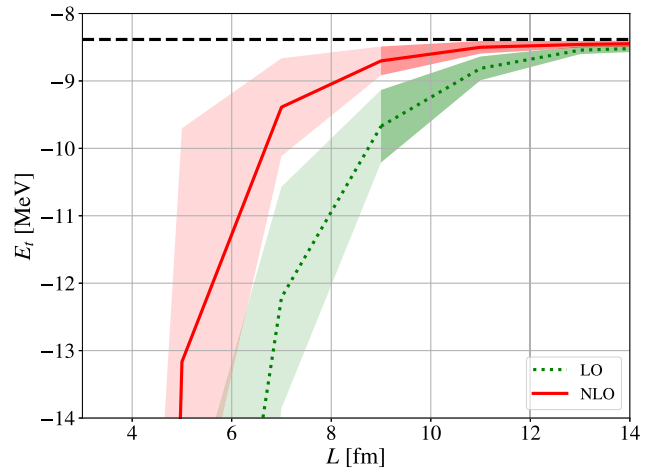


FIG. 6. Same as the upper panel of Fig. 3 but for the free-space triton bound state energy  $E_t$ .



the Minnesota triton ground state energy with increasing  $L$  and they reach an accuracy of  $\sim 4\%$  when box size  $L = 9$  fm is utilized.

The triton calculation employs the full set of two- and three-body LO and NLO LECs all of which fitted to the finite-volume data which correspond to the relatively low free-space momenta. Since the finite-volume triton ground-state energy begins to exceed the breakdown scale of the  $\not\{EFT}$  for  $L \lesssim 8$  fm (roughly estimated in Sec. IV B), the three-body LECs fit is the most limiting factor in our finite-volume study. In this small  $L$ -range the calculated  $E_t$  energies, both at LO and NLO, quickly diverge with decreasing  $L$  from the free-space Minnesota value (see lighter shaded bands in Fig. 6). As the box size gets smaller, also the two-body LECs start to gradually introduce momenta above the breakdown scale of the theory. This probably leads to a more pronounced and faster deterioration of our three-body results than in the previous two-body studies.

The lowest breakup threshold of the triton is into deuteron and neutron. Consequently, if one treats the deuteron as a pointlike particle, Eq. (2) holds. Thus, in principle, having two triton finite-volume ground state energies at two different box sizes one can constrain the parameters  $\kappa_3$  and  $\mathcal{A}_3$  in the equation and extract the free-space  $E_t$ . This is the case in the second fitting scenario. The  $E_t$  results obtained through this fit in two adjacent box sizes can be found in Appendix B. There, the corresponding  $\not\{EFT}$  triton results as well as free-space  $E_t$  energies obtained using the Lüscher-like formula, Eq. (2) are depicted in Fig. 10. It can be seen that the NLO  $\not\{EFT}$  and the Lüscher-like results converge very similarly, and both provide accurate results when average box sizes  $\langle L \rangle \gtrsim 10$  fm are used.

#### D. Three-nucleon $S = 3/2, I = 1/2$ channel

The  $S, I = 3/2, 1/2$  three-body channel does not support a bound state, and so we focus solely on the  $s$ -wave  $nd$  scattering. The scattering parameters calculated directly from the Minnesota potential are

$$a_{nd}^{3/2} \simeq 6.327 \text{ fm}, \quad r_{nd}^{3/2} \simeq 1.968 \text{ fm}.$$

This channel serves as a noteworthy demonstration of a significant advantage of the EFT. While the Lüscher approach can relate the finite-volume results to the corresponding free-space quantity and cannot predict properties of different systems based on results from another one, the EFT offers a more versatile solution. By calibrating the EFT using empirical data, it possesses the predictive power to address different characteristics of a variety of bound or unbound nuclear systems. Using fitted  $\not\{EFT}$  up to NLO, which has been employed up to now, no further finite-volume results are required, and the properties of the  $s$ -wave  $nd$  spin-quartet scattering are a pure prediction.

To this end, we solve the  $nd$  system with the harmonic potential added to the  $\not\{EFT}$  potential, resulting in a spectrum of bound states. Scattering information can then be extracted from the fitting condition relating the phase shifts of the  $s$ -wave  $\delta_{nd}^{3/2}(k)$  to the corresponding bound-state energy spectrum in the trap [51]

$$k \cot [\delta_{nd}^{3/2}(k)] = -\sqrt{4\mu_{nd}\omega} \frac{\Gamma(3/4 - \epsilon_\omega/2\omega)}{\Gamma(1/4 - \epsilon_\omega/2\omega)}. \quad (17)$$

Here  $k$  stands for the relative  $nd$  momentum and  $\mu_{nd} \simeq 2m/3$  is the respective reduced mass.  $\epsilon_\omega = E_\omega(nd) - E_\omega(d)$  is the energy of the trapped  $nd$  state with respect to the  $d$  energy threshold. Taking the limit of vanishing trapping potential, one can minimize the trap effect and obtain pure free-space results. This method has been used before, for example in Refs. [35,36,52], and has the advantage of obtaining scattering properties with a method intended for bound state calculations.

The  $\not\{EFT}$  results for the  $nd$  spin-quartet scattering parameters are shown in Fig. 7. It is apparent that the inclusion of NLO terms significantly decreases the residual cutoff dependence and shifts predicted  $a_{nd}^{3/2}$  and  $r_{nd}^{3/2}$  parameters closer to the exact Minnesota values. Only spin-triplet LO and NLO terms contribute in the  $s$ -wave  $nd$  spin-quartet channel. Consequently, the results depicted with the dotted lines reveal the same  $L$ -region, as in the Figs. 3 and 4, where the LO or NLO LECs are fitted to the finite-volume energies corresponding to the free-space momenta above the one-pion-exchange threshold.

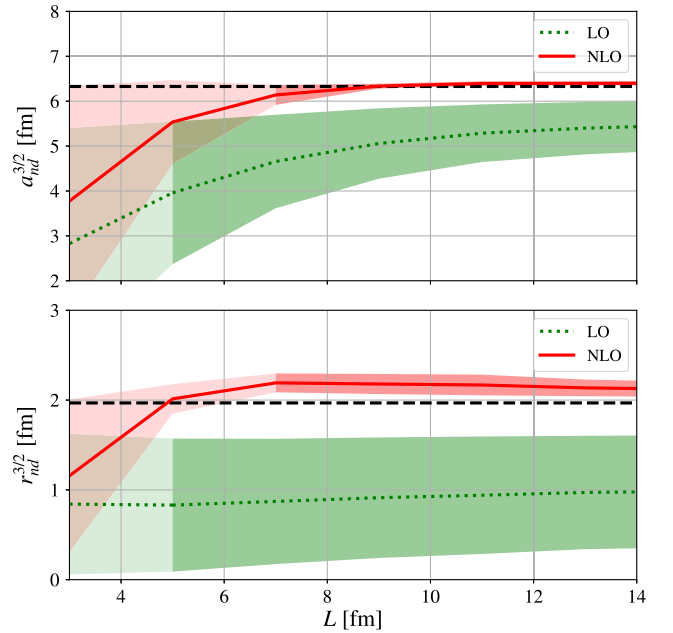


FIG. 7. Same as the upper panel of Fig. 3 but for the  $nd$  spin-quartet scattering length (upper panel) and effective range (lower panel).

TABLE I. The two-body free-space results in the deuteron and dineutron channels. We compare the results calculated directly from the Minnesota potential to those extracted from boxes of size  $L = 5$  fm and 7 fm using the Lüscher formulas, Eqs. (1) and (3), and utilizing NLO  $\not\epsilon$ EFT. The errors in the parenthesis correspond to propagated finite-volume input data uncertainties (for a detailed explanation see the text).

	Minnesota	$L = 5$ fm		$L = 7$ fm	
		Lüscher	NLO	Lüscher	NLO
$E_d$ [MeV]	-2.2	-0.8(7)	-2.5(8)	-1.8(4)	-2.2(4)
$a_{NN}^1$ [fm]	5.4	8.4(3.1)	6.1(8)	5.9(5)	6.3(6)
$r_{NN}^1$ [fm]	1.7	2.1(3)	1.8(1)	1.9(2)	2.0(2)
$1/a_{NN}^0$ [fm $^{-1}$ ]	-0.058	-0.4(3)	-0.02(2)	-0.11(5)	-0.05(2)
$r_{NN}^0$ [fm]	2.885	5.8(3.2)	2.3(2)	4(1)	2.7(3)

### E. Propagation of finite-volume data uncertainties to extrapolated results

After obtaining the results described in the previous subsections, we evaluate the robustness of the Lüscher and NLO  $\not\epsilon$ EFT approaches by examining how the uncertainties in the artificial finite-volume LQCD input data affect the free-space results. This evaluation is necessary given the possible large statistical uncertainties in LQCD results, which arise from the signal-to-noise problem in the corresponding calculations.

In the first step, we assume a relative uncertainty of 5% for the input finite-volume energies. In the second step, we propagate these uncertainties into our free-space results: For the Lüscher approach, we use analytical derivatives, while for the  $\not\epsilon$ EFT approach, we perform a Monte Carlo simulation. For simplicity, we restrict this study only to the two-body sector with  $\not\epsilon$ EFT LECs fitted through the first scenario. We use one cutoff value  $\Lambda = 4$  fm $^{-1}$  and we consider two different box sizes  $L = 5$  fm and 7 fm.

In Table I, we summarize the calculated free-space deuteron bound state energy, scattering lengths, and effective ranges with the propagated uncertainties given in the parenthesis. Using LECs fitted in the  $L = 5$  fm finite-volume, the  $\not\epsilon$ EFT  $E_d$  result has a relative uncertainty of 30%. Considering the same  $L = 5$  fm finite-volume energies, the Lüscher result has a relative uncertainty of about 85%. On the other hand, for  $L = 7$  fm, both the Lüscher result and the  $\not\epsilon$ EFT predictions for the spin-triplet scattering length and effective range show a relative uncertainty of about 9%. There is an exceptional case in the dineutron channel for  $L = 5$  fm, where the  $\not\epsilon$ EFT prediction has a larger relative uncertainty compared to the Lüscher. Nevertheless, both uncertainties remain substantial and exceed 50%. Based on the table, it is visible that the Lüscher results have either larger or comparable relative uncertainty to the corresponding NLO  $\not\epsilon$ EFT predictions.

The propagated uncertainty in the Lüscher predictions can be attributed to the behavior of the  $S(\eta)$  function in Eq. (4) that governs the prediction. Within the  $\eta$  values relevant to this study,  $S(\eta)$  changes rapidly, which means

that even small deviations from the exact value lead to different predictions. On the other hand, the  $\not\epsilon$ EFT seems to be less sensitive to the accuracy of the input data. It can be inferred that the  $\not\epsilon$ EFT might be in general more robust than the Lüscher approaches, especially when it comes to the finite-volume input data uncertainties.

## VI. CONCLUSIONS

The primary objective of this work is to explore the NLO  $\not\epsilon$ EFT with perturbative effective range corrections fitted to finite-volume input data—a crucial consideration for forthcoming LQCD calculations pertinent to nuclear physics. To achieve this, we employ both the free space and finite volume versions of the SVM, with the latter incorporating periodic boundary conditions. These few-body techniques provide us with a highly accurate framework to address the finite-volume effects at varying box sizes as well as in the free-space limit. In lieu of nuclear LQCD results at physical pion mass, and to facilitate a quantitative comparison with established data, we emulate the finite-volume spectra by solving the Minnesota  $NN$  potential.

From these finite-volume data, we extract the free-space binding energies and  $s$ -wave scattering parameters for two- and three-nucleon systems. We then juxtapose the outcomes obtained through the Lüscher methods with those derived from  $\not\epsilon$ EFT at both LO and NLO. The free-space results, which are obtained by applying directly the Minnesota potential, serve as the benchmark.

Our findings reveal a substantial improvement of  $\not\epsilon$ EFT results when transitioning from LO to NLO. Moreover, the NLO  $\not\epsilon$ EFT generally provides predictions close to the free-space Minnesota values when using the box sizes  $L \gtrsim 7$  fm. In most two-body scenarios, the NLO  $\not\epsilon$ EFT effectively captures the finite-volume effects and incorporates the necessary corrections. This trend is also evident in the  $nd$   $S = 3/2$  channel, which at NLO involves only a two-body scale. By introducing relative uncertainties into the finite-volume input data, we demonstrated the robustness of  $\not\epsilon$ EFT results. On the other hand, the Lüscher free-space results remain rather sensitive to the propagated uncertainties.

For  $L \lesssim 5$  fm, the Lüscher formalism yields the  $NN$  spin-singlet and spin-triplet  $s$ -wave phase shifts, which deviate from the corresponding free-space Minnesota values. This suggests that the finite-volume corrections in this small  $L$ -region start to be dominated by the strong interplay between the size of the box and the range of the Minnesota potential. The same might potentially affect any EFT with LECs fitted at such small box sizes. In our study, the finite-volume energies in this  $L$ -region start to correspond, through the Lüscher formalism, to  $NN$  phase shifts with momenta above the breakdown scale of  $\not\text{EFT}$ . Here, our results quickly deteriorate with decreasing  $L$  and they should be considered as a mere extrapolation outside the scope of the theory. This sets a hard limit on the validity of our  $\not\text{EFT}$  predictions.

$\not\text{EFT}$  proves to be a robust tool, not only due to its capacity to yield precise free-space results but also because it enables the extraction of meaningful insights with limited finite-volume input data. This results in a reduced number of unknown parameters that must be determined. In contrast, the Lüscher formalism demands finite volume energies from the same system to compute free space observables, while EFT offers the potential to transcend this requirement.

In future  $\not\text{EFT}$  works, it would be interesting to explore higher orders of the theory, which introduce  $p$ -wave,  $d$ -wave, and noncentral interaction terms. This would require the study of  $T_1^-$ ,  $E^+$ , and  $T_2^+$  finite-volume spectra, where the leading contribution in the  $T_1^-$  cubic symmetry is induced by the  $p$ -wave, while for the  $E^+$  and  $T_2^+$  cubic symmetries it is the  $d$ -wave. Furthermore, it is highly topical to use EFTs to explore the LQCD finite-volume results with nonzero strangeness. Here, recent advances in LQCD baryon-baryon and meson-baryon calculations [6,7,53] seem to converge rather fast to the physical pion mass. Using these LQCD results would provide an intriguing insight into a strangeness sector, where the amount of low-energy experimental data is often limited.

## ACKNOWLEDGMENTS

We would like to thank Nir Barnea and Sebastian König for useful discussions and communications. The work of M. Schäfer was supported by the Czech Science Foundation GAČR Grant No. 22-14497S.

## APPENDIX A: FINITE-VOLUME DATA

The finite-volume input data are generated using the Minnesota  $NN$  potential [43] with mixing parameter  $u = 1$ . In Table II, we list the calculated energies of the two lowest lying states of the  $A_1^+$  deuteron and dineutron spectra for different  $L$ . The finite-volume ground-state energies in the triton channel are given as well. In our calculations, we use the nucleon mass parameter  $(\hbar c)^2/m \simeq 41.471$  MeV.fm<sup>2</sup>.

## APPENDIX B: ADDITIONAL RESULTS

We introduced two different options of how to fit LO and NLO  $\not\text{EFT}$  LECs to finite-volume data (see Sec. IV B). The first scenario uses the finite-volume ground state and the first excited state energy values at the same single box size  $L$ , while the second scenario considers only the finite-volume ground state energies from two adjacent box sizes  $\langle L \rangle \pm 1$  fm. For free-space deuteron bound state energy  $E_d$  we show the corresponding  $\not\text{EFT}$  results of both fitting methods in Sec. VA. For completeness, we enclose in this appendix additional results obtained with the second fitting scheme using two adjacent box sizes.

The results of  $NN$   $s$ -wave scattering parameters are shown for spin-triplet, Fig. 8, and spin-singlet, Fig. 9. Lüscher's scattering formula, Eq. (3), can also be used here, and its results are shown as well. The free-space triton bound state energy is given in Fig. 10. In the same figure, we show the results of the generalization of Lüscher's bound state formula, Eq. (2), as well. Finally, the  $s$ -wave  $nd$  spin-quartet scattering parameters are presented in Fig. 11.

TABLE II. Finite-volume input data which are employed to constrain the  $\not\text{EFT}$  LO and NLO LECs. Listed are the ground-state ( $E_0$ ) and the first excited state ( $E_1$ )  $A_1^+$  energies in the deuteron and dineutron channels as well as the  $A_1^+$  ground-state energy value in the triton channel, which are calculated at different box sizes  $L$ . The last row of the table corresponds to the free-space results.

$L$ [fm]	Deuteron		Dineutron		Triton
	$E_0$	$E_1$	$E_0$	$E_1$	$E_0$
3	-49.6002	145.0738	-38.4197	161.5753	-131.7462
5	-13.2650	48.8501	-8.5695	60.2897	-32.8364
7	-6.8728	20.3600	-3.6048	27.9261	-16.5174
9	-4.5895	10.1385	-1.9741	15.5872	-11.3680
11	-3.5205	5.6454	-1.2355	9.8703	-9.4258
13	-2.9523	3.3794	-0.8396	6.8068	-8.7281
15	-2.6326	2.1290	-0.6036	4.9852	-8.4973
$\infty$	-2.2019	0	0	0	-8.3850

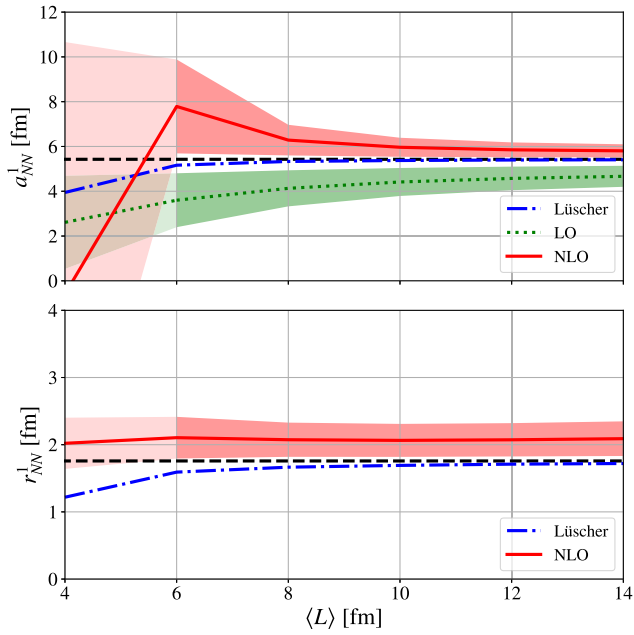


FIG. 8. Same as the lower panel of Fig. 3 but for the  $NN$  spin triplet scattering length (upper panel) and effective range (lower panel).

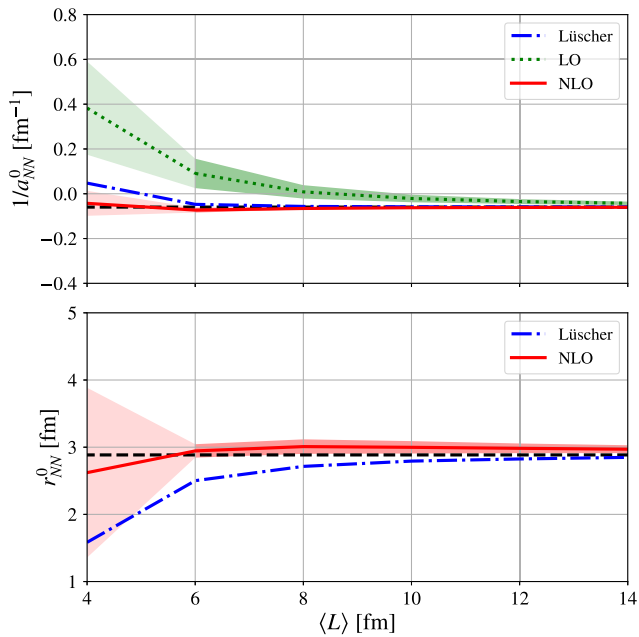


FIG. 9. Same as the lower panel of Fig. 3 but for the  $NN$  inverse spin-singlet scattering length (upper panel) and effective range (lower panel).

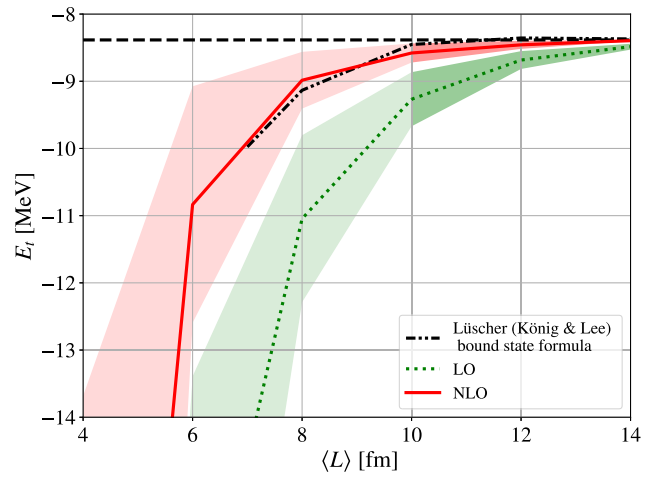


FIG. 10. Same as the lower panel of Fig. 3 but for the free-space triton ground state energy  $E_t$ . Here, the black dash-double dotted line show  $E_t$  results obtained through the generalized Lüscher bound state formula, Eq. (2).

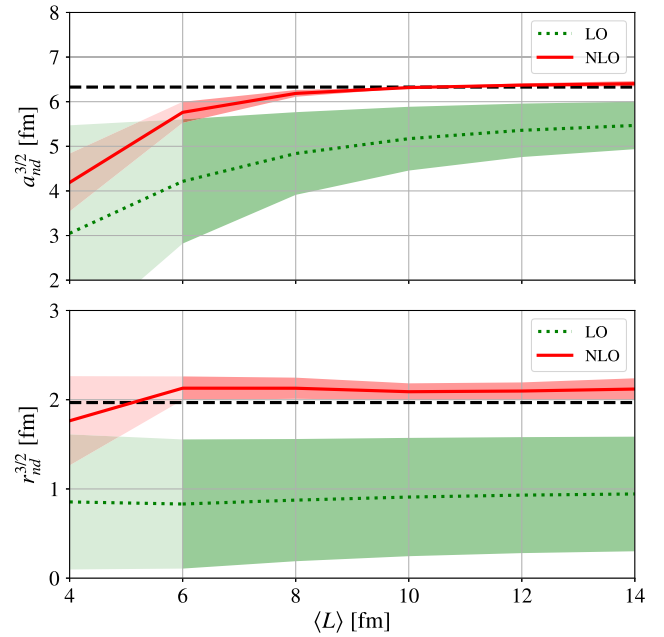


FIG. 11. Same as the lower panel of Fig. 3 but for the  $nd$  spin-quartet scattering length (upper panel) and effective range (lower panel).

- [1] K. G. Wilson, Confinement of quarks, *Phys. Rev. D* **10**, 2445 (1974).
- [2] S. Amarasinghe, R. Baghdadi, Z. Davoudi, W. Detmold, M. Illa, A. Parreño, A. V. Pochinsky, P. E. Shanahan, and M. L. Wagman, A variational study of two-nucleon systems with lattice QCD *Phys. Rev. D* **107**, 094508 (2023).
- [3] J. R. Green, A. D. Hanlon, P. M. Junnarkar, and H. Wittig, Weakly bound H dibaryon from SU(3)-flavor-symmetric QCD, *Phys. Rev. Lett.* **127**, 242003 (2021).
- [4] T. Yamazaki, K.-I. Ishikawa, Y. Kuramashi, and A. Ukawa, Study of quark mass dependence of binding energy for light nuclei in  $2 + 1$  flavor lattice QCD, *Phys. Rev. D* **92**, 014501 (2015).
- [5] E. Berkowitz, T. Kurth, A. Nicholson, B. Joó, E. Rinaldi, M. Strother, P. M. Vranas, and A. Walker-Loud, Two-nucleon higher partial-wave scattering from lattice QCD, *Phys. Lett. B* **765**, 285 (2017).
- [6] T. Iritani *et al.* (HAL QCD Collaboration),  $N\Omega$  dibaryon from lattice QCD near the physical point, *Phys. Lett. B* **792**, 284 (2019).
- [7] K. Sasaki *et al.* (HAL QCD Collaboration),  $\Lambda\Lambda$  and  $N\Xi$  interactions from lattice QCD near the physical point, *Nucl. Phys. A* **998**, 121737 (2020).
- [8] M. Lüscher, Volume dependence of the energy spectrum in massive quantum field theories. I. Stable particle states, *Commun. Math. Phys.* **104**, 177 (1986).
- [9] M. Lüscher, Volume dependence of the energy spectrum in massive quantum field theories. II. Scattering states, *Commun. Math. Phys.* **105**, 153 (1986); Two-particle states on a torus and their relation to the scattering matrix, *Nucl. Phys. B* **354**, 531 (1991).
- [10] Z. Davoudi and M. J. Savage, Improving the volume dependence of two-body binding energies calculated with lattice QCD, *Phys. Rev. D* **84**, 114502 (2011).
- [11] I. Sato and P. F. Bedaque, Fitting two nucleons inside a box: Exponentially suppressed corrections to Lüscher's formula, *Phys. Rev. D* **76**, 034502 (2007).
- [12] R. A. Briceno and Z. Davoudi, Three-particle scattering amplitudes from a finite volume formalism, *Phys. Rev. D* **87**, 094507 (2013).
- [13] M. T. Hansen and S. R. Sharpe, Relativistic, model-independent, three-particle quantization condition, *Phys. Rev. D* **90**, 116003 (2014).
- [14] M. T. Hansen and S. R. Sharpe, Expressing the three-particle finite-volume spectrum in terms of the three-to-three scattering amplitude, *Phys. Rev. D* **92**, 114509 (2015).
- [15] U.-G. Meissner, G. Rios, and A. Rusetsky, Spectrum of three-body bound state in a finite volume, *Phys. Rev. Lett.* **114**, 091602 (2015).
- [16] R. A. Briceno, M. T. Hansen, and S. R. Sharpe, Relating the finite-volume spectrum and the two-and-three-particle S matrix for relativistic systems of identical scalar particles, *Phys. Rev. D* **95**, 074510 (2017).
- [17] H.-W. Hammer, J. Y. Pang, and A. Rusetsky, Three-particle quantization condition in a finite volume: 1. The role of the three-particle force, *J. High Energy Phys.* **09** (2017) 109.
- [18] H.-W. Hammer, J. Y. Pang, and A. Rusetsky, Three-particle quantization condition in a finite volume: 2. General formalism and the analysis of data, *J. High Energy Phys.* **10** (2017) 115.
- [19] M. Mai and M. Döring, Three-body unitarity in the finite volume, *Eur. Phys. J. A* **53**, 240 (2017).
- [20] S. König and D. Lee, Volume dependence of N-body bound states, *Phys. Lett. B* **779**, 9 (2018).
- [21] S. König, Few-body bound states and resonances in finite volume, *Few-Body Syst.* **61**, 20 (2020).
- [22] H. Yu, S. König, and D. Lee, Charged-particle bound states in periodic boxes, *Phys. Rev. Lett.* **131**, 212502 (2023).
- [23] M. Elyahu, B. Bazak, and N. Barnea, Extrapolating lattice QCD results using effective field theory, *Phys. Rev. C* **102**, 044003 (2020).
- [24] H.-W. Hammer, S. König, and U. van Kolck, Nuclear effective field theory: Status and perspectives, *Rev. Mod. Phys.* **92**, 025004 (2020).
- [25] D. B. Kaplan, M. J. Savage, and M. B. Wise, A new expansion for nucleon-nucleon interactions, *Phys. Lett. B* **424**, 390 (1998).
- [26] P. F. Bedaque, H.-W. Hammer, and U. van Kolck, Effective theory for neutron-deuteron scattering: Energy dependence, *Phys. Rev. C* **58**, R641(R) (1998).
- [27] U. van Kolck, Effective field theory of short-range forces, *Nucl. Phys. A* **645**, 273 (1999).
- [28] M. C. Birse, J. A. McGovern, and K. G. Richardson, A renormalisation-group treatment of two-body scattering, *Phys. Lett. B* **464**, 169 (1999).
- [29] S. R. Beane, E. Chang, S. D. Cohen, W. Detmold, H. W. Lin, T. C. Luu, K. Orginos, A. Parreño, M. J. Savage, and A. Walker-Loud (NPLQCD Collaboration), Light nuclei and hypernuclei from quantum chromodynamics in the limit of SU(3) flavor symmetry, *Phys. Rev. D* **87**, 034506 (2013).
- [30] A. Parreño, P. E. Shanahan, M. L. Wagman, F. Winter, E. Chang, W. Detmold, and M. Illa (NPLQCD Collaboration), Axial charge of the triton from lattice QCD, *Phys. Rev. D* **103**, 074511 (2021).
- [31] W. Detmold and P. E. Shanahan, Few-nucleon matrix elements in pionless effective field theory in a finite volume, *Phys. Rev. D* **103**, 074503 (2021).
- [32] Z. Davoudi and S. V. Kadam, Extraction of low-energy constants of single- and double- $\beta$  decays from lattice QCD: A sensitivity analysis, *Phys. Rev. D* **105**, 094502 (2022).
- [33] W. Detmold, F. Romero-López, and P. E. Shanahan, Constraint of pionless EFT using two-nucleon spectra from lattice QCD, *Phys. Rev. D* **108**, 034509 (2023).
- [34] J. Vannasse, Fully perturbative calculation of  $nd$  scattering to next-to-next-to-leading order, *Phys. Rev. C* **88**, 044001 (2013).
- [35] M. Schäfer and B. Bazak, Few-nucleon scattering in pionless effective field theory, *Phys. Rev. C* **107**, 064001 (2023).
- [36] M. Bagnarol, M. Schäfer, B. Bazak, and N. Barnea, Five-body calculation of s-wave n-4He scattering at next-to-leading order pionless EFT, *Phys. Lett. B* **844**, 138078 (2023).
- [37] M. Ebert, H.-W. Hammer, and A. Rusetsky, An alternative scheme for effective range corrections in pionless EFT, *Eur. Phys. J. A* **57**, 332 (2021).
- [38] M. Ebert, H.-W. Hammer, and A. Rusetsky, An alternative scheme for pionless EFT: Neutron-deuteron scattering in the doublet S-wave, *Few-Body Syst.* **64**, 87 (2023).
- [39] E. P. Wigner, Lower limit for the energy derivative of the scattering phase shift, *Phys. Rev.* **98**, 145 (1955).

- [40] D. Phillips, R. Cohen, and D. Thomas, How short is too short? Constraining contact interactions in nucleon-nucleon scattering, *Phys. Lett. B* **390**, 7 (1997).
- [41] X. Yin and D. Blume, Small two-component Fermi gases in a cubic box with periodic boundary conditions, *Phys. Rev. A* **87**, 063609 (2013).
- [42] R. Yaron, B. Bazak, M. Schäfer, and N. Barnea, Spectrum of light nuclei in a finite volume, *Phys. Rev. D* **106**, 014511 (2022).
- [43] D. R. Thompson, M. Lemere, and Y. C. Tang, Systematic investigation of scattering problems with the resonating-group method, *Nucl. Phys. A* **286**, 53 (1977).
- [44] S. R. Beane, P. F. Bedaque, A. Parreño, and M. J. Savage, Two nucleons on a lattice, *Phys. Lett. B* **585**, 106 (2004).
- [45] B. Bazak, J. Kirscher, S. König, M. Pavón Valderrama, N. Barnea, and U. van Kolck, Four-body scale in universal few-boson systems, *Phys. Rev. Lett.* **122**, 143001 (2019).
- [46] H. W. Griesshammer, A consistency test of EFT power countings from residual cutoff dependence, *Eur. Phys. J. A* **56**, 118 (2020).
- [47] Y. Suzuki and K. Varga, *Stochastic Variational Approach to Quantum-Mechanical Few-Body Problems* (Springer, Berlin, 1998).
- [48] K. Varga and Y. Suzuki, Precise solution of few body problems with stochastic variational method on correlated Gaussian basis, *Phys. Rev. C* **52**, 2885 (1995).
- [49] J. E. Mandula, G. Zweig, and J. Govaerts, Representations of the rotation reflection symmetry group of the four-dimensional cubic lattice, *Nucl. Phys. B* **228**, 91 (1983).
- [50] F. Romero-López, S. R. Sharpe, T. D. Blanton *et al.*, Numerical exploration of three relativistic particles in a finite volume including two-particle resonances and bound states, *J. High Energy Phys.* **10** (2019) 007.
- [51] T. Busch, B. G. Englert, K. Rzazewski, and M. Wilkens, Two cold atoms in a harmonic trap, *Found. Phys.* **28**, 549 (1998).
- [52] J. Rotureau, I. Stetcu, B. R. Barrett, and U. van Kolck, Two and three nucleons in a trap, and the continuum limit, *Phys. Rev. C* **85**, 034003 (2012).
- [53] J. Bulava *et al.*, Lattice QCD study of  $\pi\Sigma - K^-N$  scattering and the  $\Lambda(1405)$  resonance, *Phys. Rev. D* **109**, 014511 (2024).